17. Bezryadin, A., Dekker, C. & Schmid, G. Electrostatic trapping of single conducting nanoparticles between nanoelectrodes. *Appl. Phys. Lett.* **71**, 1273–1275 (1997).

18. Graybeal, J. M. & Beasley, M. R. Localization and interaction effects in ultrathin amorphous superconducting films. *Phys. Rev. B* **29**, 4167–4169 (1984).

19. Oreg, Y. & Finkelstein, A. M. Suppression of T_c in superconducting amorphous wires. *Phys. Rev. Lett.* **83**, 191–194 (1999).

20. Goldman, A. M. & Marković, N. Superconductor-insulator transition in the two-dimensional limit. *Phys. Today* **51**, 39–44 (1998).

21. Mooij, J. E. & Schön, G. Propagating plasma mode in thin superconducting filaments. *Phys. Rev. Lett.* **55**, 114–117 (1985).

....

Measurement of the quantum of thermal conductance

K. Schwab*, E. A. Henriksen*, J. M. Worlock*† & M. L. Roukes*

* *Condensed Matter Physics 114-36, California Institute of Technology, Pasadena, California 91125, USA*

....

The physics of mesoscopic electronic systems has been explored for more than 15 years. Mesoscopic phenomena in transport processes occur when the wavelength or the coherence length of the carriers becomes comparable to, or larger than, the sample dimensions. One striking result in this domain is the quantization of electrical conduction, observed in a quasi-one-dimensional constriction formed between reservoirs of two-dimensional electron gas[1,2]. The conductance of this system is determined by the number of participating quantum states or 'channels' within the constriction; in the ideal case, each spin-degenerate channel contributes a quantized unit of $2e^2/h$ to the electrical conductance. It has been speculated that similar behaviour should be observable for thermal transport[3,4] in mesoscopic phonon systems. But experiments attempted in this regime have so far yielded inconclusive results[5–9]. Here we report the observation of a quantized limiting value for the thermal conductance, G_{th}, in suspended insulating nanostructures at very low temperatures. The behaviour we observe is consistent with predictions[10,11] for phonon transport in a ballistic, one-dimensional channel: at low temperatures, G_{th} approaches a maximum value of $g_0 = \pi^2 k_B^2 T/3h$, the universal quantum of thermal conductance.

The thermal conductance of phonon waveguides in the ballistic, one-dimensional limit has recently been calculated using the Landauer formula[10–12]. This approach, which bears a formal similarity to the model developed for radiative thermal transport in solids[13], leads to an expression for the reservoir-to-reservoir heat current J_{th} that takes the form:

$$J_{th} = \sum_m \int_0^\infty \frac{dk}{2\pi} \hbar\omega_m(k) v_m(k) [\eta_{hot} - \eta_{cold}] T_m(k) \quad (1)$$

Here m is the mode index, $\omega_m(k)$ is the phonon dispersion relation for wavevector k, $v_m(k)$ is the group velocity, $\eta = [\exp(\hbar\omega_m/k_B T) - 1]^{-1}$ are Bose–Einstein occupation factors for the two (hot/cold) thermal reservoirs connected by the phonon

† Present address: Department of Physics, University of Utah, Salt Lake City, Utah 84112, USA

waveguides, and $T_m(k)$ are transmission coefficients characterizing the coupling of waveguide modes to these reservoirs. As for the case with electrons, conversion to an integral over energy, $\hbar\omega$, leads to a cancellation between the density of states $\partial k/\partial\omega_m$ and the modal group velocity, $v_m(k)$. In the limit of linear response, $\Delta T \ll T$, the resulting expression for thermal conductance depends only upon $T_m(\omega)$, the mode thresholds at $q = 0$ (labelled ω_m), and fundamental constants:

$$G_{th} = \frac{J_{th}}{\Delta T} = \frac{k_B^2}{h} \sum_m \int_{x_m}^\infty dx \frac{x^2 e^x}{(e^x - 1)^2} T_m(x k_B T/\hbar) \quad (2)$$

Here, ΔT is the small, steady-state temperature difference between reservoirs that sustains J_{th} and $x_m = \hbar\omega_m(k=0)/k_B T$.

This expression becomes greatly simplified in the limit $k_B T \le \hbar\omega_m$, where only the four lowest lying, massless modes (that is, having zero threshold, $\hbar\omega_i(k=0) = 0$) make an appreciable contribution. These four lowest modes arise from one dilatational, one torsional, and two flexural degrees of freedom[14]. For ideal coupling between the ballistic thermal conductor and the reservoirs, yielding modal transmission coefficients, T_m, equal to unity, a fundamental relation holds for each mode,

$$G_{th} = g_0 = \pi^2 k_B^2 T/(3h) \quad (3)$$

an expression devoid of any material parameters. This quantum of thermal conductance, $g_0 = (9.456 \times 10^{-13} \text{ W/K}^2)T$, represents the maximum possible value of energy transported per phonon mode. Surprisingly, it does not depend on particle statistics—but is universal for fermions, bosons and anyons[15,16]. A connection exists between the maximum thermal conductance and the maximum rate at which information, or entropy, can flow in a single quantum channel[3,17].

Electrical and thermal conductance quantization are manifestly different in a number of ways; we discuss here two that are most obvious. The factor of T in equation (3), which gives the thermal conductance quantum a linear dependence upon temperature, reflects the fact that the quantity transported is energy (that is, entropy). In the case of electronic conduction, the corresponding quantity is the electron charge, e, and the electrical conduction quantum per spin-degenerate band is temperature independent, $g_0^{el} = 2e^2/h$. Also, in experiments with electrons, a series of conductance steps is observed[1,2]. In such experiments, chemical potential and temperature can be controlled separately. At a fixed, low temperature, the edge of the sharp electron distribution function can be swept sequentially through one-dimensional modes. With phonons, we can sweep only temperature; in this case, the broader Bose distribution smears out all features except for the final low-temperature plateau which occurs only when all but the lowest-lying modes become thermally depopulated[10,11].

There are three essential criteria for observing the thermal conductance quantum. First, ballistic phonon transport through one-dimensional 'waveguides' is required. Second, as described below, coupling between the lowest modes and the thermal reservoirs must be optimal over an appreciable temperature range (their transmission coefficients must remain close to unity). Finally, the sample configuration and measurement technique must provide sufficient resolution to observe the contribution to G_{th} from a single mode.

To satisfy these criteria, we have developed new fabrication techniques based on the initial work of Tighe et al.[18] on thermally isolated mesoscopic samples with integrated transducers. Figure 1 shows a representative sample, which includes a phonon 'cavity' (a quasi-isolated thermal reservoir) suspended by four phonon 'waveguides'. These are fabricated from a 60-nm-thick silicon nitride membrane by electron beam lithography and pattern transfer techniques described elsewhere[19]. In the earlier work, Tighe et al. fabricated devices from a GaAs layer that was monocrystalline. This

is not the case for the silicon nitride structural layer employed here; however, this material does provide a homogeneous effective medium for the long-wavelength phonons of relevance to these experiments. Recent measurements have shown that phonon propagation in this material is ballistic at low temperatures[20,21].

Motivated by idealized scalar-wave calculations for an isotropic elastic solid of comparable geometry and dimensions[11], we have patterned the width of the waveguides to follow $\cosh^2(x/\lambda)$, where x is the longitudinal coordinate and $\lambda = 1.0\,\mu m$. The calculations, valid for longitudinal wave propagation through waveguides of this shape, indicate that quantized thermal conductance may be observable over an appreciable temperature range; this range is bounded at low temperatures by loss of adiabatic coupling to the reservoirs and, at higher temperatures, by the onset of thermal population of higher-energy (massive) modes.

Integration of carefully designed transducers allows thermal conductance measurements on the nanoscale phonon waveguides. We realize these by patterning (from a 25-nm-thick Au film) two thin-film resistors on top of the phonon cavity. As described below, these serve as a local heater and thermometer for the measurements; a second thermometer measures substrate temperature. Electrical connection to these transducers is provided by thin-film Nb leads (thickness 25 nm) patterned above the waveguides; these extend from the cavity to wirebond pads anchored to the main part of the chip. By virtue of their superconductivity, these leads do not provide a parasitic thermalization path to the reservoirs.

In principle, the measurement technique is simple—we first raise the temperature of the phonon cavity by Joule-heating its integrated Au resistor. We then employ the second transducer to measure the induced change in temperature. The ratio of heat current flowing through the waveguides to the induced rise in cavity temperature is the phonon thermal conductance of the waveguides. In practice, however, this measurement is quite challenging—it is necessary to obtain a sensitive measurement of phonon temperature within a suspended nanostructure that has very small heat capacity. The measurement process itself must involve minimal power dissipation, because exceedingly weak coupling exists between the sensor electrons and the cavity phonons at very low temperatures ($10^{-13}\,W\,K^{-1}$ at 100 mK for $0.1\,\mu m^3$ of Au)[22]. As depicted in Fig. 2, we employ d.c. SQUID-based noise thermometry[23,24] to measure the
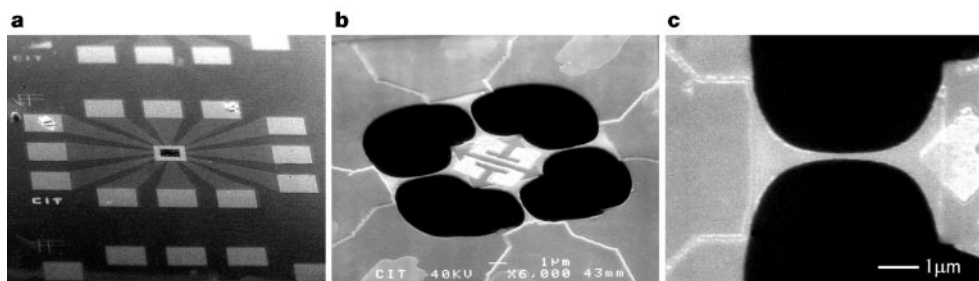

Figure 1 Suspended mesoscopic device. A series of progressive magnifications are shown. **a**, Overall view of the ~1.0 × 0.8 mm device, showing 12 wirebond pads that converge via thin-film niobium leads into the centre of the device. This central region is a 60-nm-thick silicon nitride membrane, which appears dark in the electron micrograph. **b**, View of the suspended device, which consists of a 4 × 4 μm 'phonon cavity' (centre) patterned from the membrane. In this view, the bright ''c'' shaped objects on the device are thin-film gold transducers, whereas in the dark regions the membrane has been completely removed. The transducers are connected to thin-film. niobium leads that run atop the 'phonon waveguides'; these leads ultimately terminate at the wirebond pads. **c**, Close-up of one of the catenoidal waveguides, displaying the narrowest region which necks down to <200-nm width.
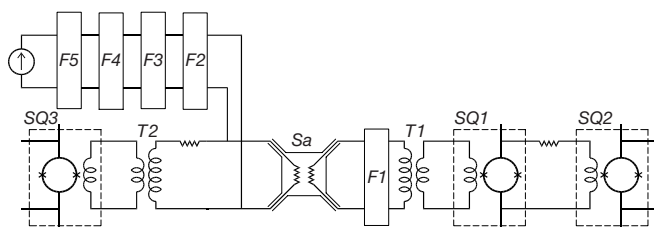
Figure 2 Simplified apparatus diagram. The suspended sample (Sa), cooled on the dilution refrigerator's mixing chamber (MC), is represented by two (~20 Ω) resistors in the centre of the figure. Its rightmost (sensor) transducer is coupled to a d.c. SQUID-based noise thermometry circuit. Two thin-film d.c. SQUIDs (SQ1, SQ2) are cooled on the MC to enable ultralow noise performance: SQ1 is run open-loop (with continuous gain measurement carried out at 900 Hz, that is, just outside the noise measurement band) while its readout, SQ2, is operated in flux-locked mode. The metallic powder filter (F1) on the MC shields the sample from Josephson radiation emanating from the SQUIDs. The sample's leftmost (heater) transducer is connected to a heavily filtered (F2–F5) current biasing circuit used to Joule-heat the phonon cavity. A SQUID voltmeter circuit (SQ3) on the MC allows resistance measurement *in situ*, by sensing the voltage drop across the current biased heater. The heavily shielded superconducting transformers (T1, T2) provide a current gain of ~18. The cold sample is isolated from heat conduction from the higher-temperature environment through filters F2 and F3 (cooled on the MC) and F4 and F5 (at 700 mK). F2 and F4 are metallic powder filters, while F3 and F5 are 10-pole *RC* filters.
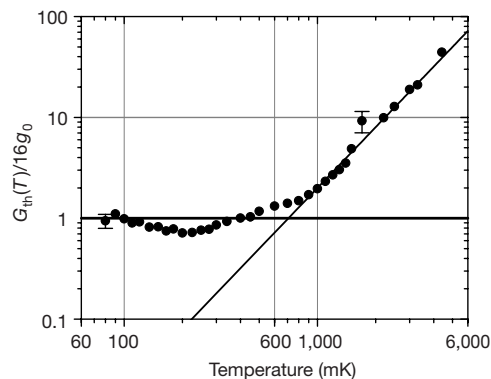
Figure 3 Thermal conductance data. We normalize the measured thermal conductance by the expected low-temperature value for 16 occupied modes, 16 g_0. Measurement error is approximately the size of the data points, except where indicated. For temperatures above $T_{co} \approx 0.8\,K$, we observe a cubic power-law behaviour consistent with a mean free path of ~0.9 μm. For temperatures below T_{co}, we observe a saturation in G_{th} at a value near the expected quantum of thermal conductance. Consistent with expectations, to within experimental uncertainty, G_{th} never exceeds 16 g_0 once it finally drops below that value. The (implicit) linear temperature dependence observed for $T < T_{co}$ is the hallmark of one-dimensional thermal transport. The approximate saturation at the maximum expected magnitude, $G_{th} \approx 16\,g_0$, indicates that both the ballistic and adiabatic conditions have been satisfied in these experiments.

electron temperature within the Au film patterned on the suspended cavity. We also employ a second d.c. SQUID system to measure, *in situ*, the resistance of the transducer serving as a local heater. These d.c. SQUID devices operate with nearly quantum-limited energy sensitivity ($\sim$220h)[25], thus permitting measurement of temperature with extremely small back action, estimated to be $\sim10^{-20}$ W or smaller.

To obtain a d.c. connection from the room-temperature electronics directly to the suspended nanostructures, we have installed an extensive array of filters within the cryostat (Fig. 2). These absorb both the environmental and the Johnson noise radiated from higher temperatures and Josephson radiation from the SQUIDS, and include cryogenically-cooled 10-pole *RC*-filters and "lossy-line" filters[26]. To illustrate the challenges involved, the total available power radiated from a resistor at 1 K to one at the (coldest) sample stage on the mixing chamber of the dilution refrigerator is $\sim10^{-12}$ W, and contains significant spectral density from d.c. to frequencies of the order of 40 GHz. This is far above tolerable power levels ($\sim10^{-15}$ W) at 100 mK. The filters we have employed provide measured attenuation >200 dB from 1 MHz to 20 GHz. One set of these is installed at the still (0.7 K) to adsorb the power radiated down from 300 K, while the second bank is installed at the mixing chamber (coldest stage) to absorb the power radiated downward from the filters at 0.7 K. We estimate the maximum total power coupled to the device from room temperature is less than 10^{-18} W, even while maintaining a d.c. connection to the suspended nano-scale sample on the cold stage.

Noise thermometry is performed by integrating the noise current emanating from the sensor over a 500-Hz bandwidth centred at 1.25 kHz (Fig. 2). The measured noise power is directly proportional to temperature from >4 K down to $\sim$80 mK. Below this, the transducer electrons lose contact with the lattice[22], and the electrons remain at a temperature above that of the dilution refrigerator, presumably due to residual external noise. The observed saturation at low temperatures can be attributed to approximately 10^{-16} W of parasitic power input. This residual power is always very much smaller than the minimum level used to probe G_{th} in our experiments, which is of the order of 10^{-14} W at the lowest temperatures, and hence plays a negligible role. We note, however, that its magnitude is inconsistent with the measured attenuation of our filters, our carefully shielded environment, and the back action power of the SQUIDs. It is reminiscent of low temperature saturation in phase breaking times, and may have physical significance[27].

Figure 3 shows the measured thermal conductance, normalized to $16\,g_0$ (for reasons described below), which displays a clear saturation at low temperature. This is in striking contrast with the behaviour manifested above $\sim$1 K where a precipitous rise in G_{th}, closely following a cubic power law, is manifested. Roughly speaking, with decreasing temperature the one-dimensional limit is attained when the thermal wavevector $k_{th} = k_B T/(\hbar v)$ becomes smaller than the spacing between the lowest-lying modes, $\Delta k \sim \pi/w$. Assuming an average speed of sound $v\sim6{,}000$ m s^{-1}, depopulation of the higher-lying, massive modes should occur below a crossover temperature $T_{co}\sim\pi\hbar v/(k_B w) = 0.8$ K for our waveguides of width $w \approx 200$ nm. Thus, with the phonon cavity cooled via four waveguides that are each expected to carry just four populated modes at the lowest temperatures, G_{th} should approach a limiting value of $16\,g_0$ for $T \ll T_{co}$, as is found. Some structure is evident as temperature is decreased below 1 K but, significantly, once g becomes smaller than $16\,g_0$, to within experimental uncertainty, the data never exceed this value again. In this regime, $16\,g_0$ represents the maximum theoretical conductance; it can be attained only with perfect coupling to the reservoirs. Deviations from exact quantization here are reminiscent of those generic to the case of electrical conduction quantization which are ubiquitous, and can be induced by disorder, non-adiabatic coupling to the reservoirs, and scattering at the threshold of transmission to higher channels[28,29]. In the present case, they may

also arise from the transition from specular to diffuse phonon scattering at the waveguide surfaces that is expected at elevated temperatures[18]. Additional experiments are currently underway to clarify these details.

These devices offer prospects for extremely sensitive calorimetry. We estimate that their total heat capacity at 100 mK, dominated by the electronic contribution from Au transducers, is of the order of $C_{tot} \approx 10^3\,k_B$. We are currently attempting to measure C_{tot} directly. Our future investigations will focus upon nanocalorimeters with electron-gas transducers patterned from an $n(+)$ GaAs epilayer, rather than thin-film Au as in this work. This may allow us to obtain values of C_{tot} of a few times Boltzmann's at 10 mK. Reading out such devices with the d.c. SQUID techniques developed for this work would yield energy sensitivity sufficient to count individual thermal phonons in the 10–100 mK regime. This level of sensitivity should allow access to a regime where it may be possible to observe the particle nature of the phonons; that is, quantum phonon optics[30]. □

1. van Wees, B. J. *et al.* Quantized conductance of point contacts in a two-dimensional electron-gas. *Phys. Rev. Lett.* **60**, 848–850 (1988).
2. Wharam, D. A. *et al.* One-dimensional transport and the quantization of the ballistic resistance. *J. Phys. C* **21**, L209–L214 (1988).
3. Pendry, J. B. Quantum limits to the flow of information and entropy. *J. Phys. A* **16**, 2161–2171 (1983).
4. Maynard, R. & Akkermans, E. Thermal conductance and giant fluctuations in one-dimensional disordered systems. *Phys. Rev. B* **32**, 5440–5442 (1985).
5. Lee, K. L., Ahmed, H., Kelly, M. J. & Wybourne, M. N. Fabrication of ultra-thin freestanding wires. *Phys. Rev. Lett.* **69**, 1427–1430 (1992).
6. Seyler, J. & Wyborne, M. N. Acoustic wave-guide modes observed in electrically heated metal wires. *Phys. Rev. Lett.* **69**, 1427–1430 (1992).
7. Kwong, Y. K., Lin, K., Isaacson, M. S. & Parpia, J. M. An attempt to observe phonon dimensionality crossover effects in the inelastic-scattering rate of thin freestanding aluminium films. *J. Low Temp. Phys.* **88**, 261–272 (1992).
8. Potts, A. *et al.* Thermal transport in freestanding semiconducting fine wires. *Superlatt. Microstruct.* **9**, 315–318 (1991).
9. Hone, J., Whitney, M., Piskoti, C. & Zettl, A. Thermal conductivity of single-walled carbon nanotubes. *Phys. Rev. B* **59**, R2514–R2516 (1999).
10. Angelescu, D. E., Cross, M. C. & Roukes, M. L. Heat transport in mesoscopic systems. *Superlatt. Microstruct.* **23**, 673–689 (1998).
11. Rego, L. G. C. & Kirczenow, G. Quantized thermal conductance of dielectric quantum wires. *Phys. Rev. Lett.* **81**, 232–235 (1998).
12. Blencowe, M. P. Quantum energy flow in mesoscopic dielectric structures. *Phys. Rev. B* **59**, 4992–4998 (1999).
13. Klitsner, T., VanCleve, J. E., Fischer, J. E. & Pohl, R. O. Phonon radiative heat-transfer and surface scattering. *Phys. Rev. B* **38**, 7576–7594 (1988).
14. Nishiguchi, N., Ando, Y. & Wybourne, M. N. Acoustic phonon modes of rectangular quantum wires. *J. Phys. Cond. Matter* **9**, 5751–5764 (1997).
15. Rego, L. C. G. & Kirczenow, G. Fractional exclusion statistics and the universal quantum of thermal conductance: A unifying approach. *Phys. Rev. B* **59**, 13080–13086 (1999).
16. Krive, I. V. & Mucciolo, E. R. Transport properties of quasiparticles with fractional exclusion statistics. *Phys. Rev. B* **60**, 1429–1432 (1999).
17. Caves, C. M. & Drummond, P. D. Quantum limits on bosonic communication rates. *Rev. Mod. Phys.* **66**, 481–537 (1994).
18. Tighe, T. S., Worlock, J. M. & Roukes, M. L. Direct thermal conductance measurements on suspended monocrystalline nanostructures. *Appl. Phys. Lett.* **70**, 2687–2689 (1997).
19. Schwab, K., Henriksen, E. A. & Roukes, M. L. Direct measurement of phonon transport in mesoscopic devices. *Appl. Phys. Lett.* (submitted).
20. Leivo, M. M. & Pekola, J. P. Thermal characteristics of silicon nitride membranes at sub-Kelvin temperatures. *Appl. Phys. Lett.* **72**, 1305–1307 (1998).
21. Holmes, W., Gildemeister, J. M., Richards, P. L. & Kotsubo, V. Measurements of thermal transport in low stress silicon nitride films. *Appl. Phys. Lett.* **72**, 2250–2252 (1998).
22. Roukes, M. L., Freeman, M. R., Germain, R. S., Richardson, R. C. & Ketchen, M. B. Hot-electrons and energy-transport in metals at millikelvin temperatures. *Phys. Rev. Lett.* **55**, 422–425 (1985).
23. Roukes, M. L., Germain, R. S., Freeman, M. R. & Richardson, R. C. DC SQUID noise thermometry. *Physica* **126 B+C**, 1177–1178 (1984).
24. Roukes, M. L. *Hot Electrons and Energy Transport in Metals at mK Temperatures.* Doctoral dissertation, Cornell Univ. (1985).
25. Ketchen, M. B. *et al.* Design, fabrication, and performance of integrated miniature SQUID suseptometers. *IEEE Trans. Magn.* **25**, 1212–1215 (1989).
26. Martinis, J. M., Devoret, M. H. & Clarke, J. Experimental test for the quantum behavior of a macroscopic degree of freedom: The phase difference across a Josephson junction. *Phys. Rev. B* **35**, 4682–4698 (1986).
27. Mohanty, P., Jariwala, E. M. Q. & Webb, R. A. Intrinsic decoherence in mesoscopic systems. *Phys. Rev. Lett.* **78**, 3366–3369 (1997).
28. Yacoby, A. & Imry, Y. Adiabatic mode selection and the accuracy of the quantization of conductance of ballistic point contacts. *Europhys. Lett.* **11**, 663–667 (1990).
29. Kander, I., Imry, Y. & Sivan, U. Effects of channel opening and disorder on the conductance of narrow wires. *Phys. Rev. B* **41**, 12941–12944 (1990).
30. Roukes, M. L. Yoctocalorimetry: phonon counting in nanostructures. *Physica B* **263–264** 1–15 (1999).

....

Coulomb-blockade transport in single-crystal organic thin-film transistors

W. A. Schoonveld*†, J. Wildeman†‡, D. Fichou§, P. A. Bobbert‖, B. J. van Wees*† & T. M. Klapwijk¶

* Department of Applied Physics, † Materials Science Center, ‡ Department of Polymer Chemistry, University of Groningen, Nijenborgh 4, 9747 AG Groningen, The Netherlands
§ Laboratoire des Matériaux Moléculaires, CNRS, 2 rue Henry-Dunant, 94320 Thiais, France
‖ Physics Department, Eindhoven University of Technology, PO Box 513, NL-5600 MB Eindhoven, The Netherlands
¶ Delft University of Technology, Department of Applied Physics, Nanophysics and Nanotechnology Section, Lorentzweg 1, 2628 CJ Delft, The Netherlands

..

Coulomb-blockade transport—whereby the Coulomb interaction between electrons can prohibit their transport around a circuit—occurs in systems in which both the tunnel resistance, R_T, between neighbouring sites is large ($\gg h/e^2$) and the charging energy, E_C ($E_C = e^2/2C$, where C is the capacitance of the site), of an excess electron on a site is large compared to kT. (Here e is the charge of an electron, k is Boltzmann's constant, and h is Planck's constant.) The nature of the individual sites— metallic, superconducting, semiconducting or quantum dot—is to first order irrelevant for this phenomenon to be observed[1]. Coulomb blockade has also been observed in two-dimensional arrays of normal-metal tunnel junctions[2], but the relatively large capacitances of these micrometre-sized metal islands results in a small charging energy, and so the effect can be seen only at extremely low temperatures. Here we demonstrate that organic thin-film transistors based on highly ordered molecular materials can, to first order, also be considered as an array of sites separated by tunnel resistances. And as a result of the sub-nanometre sizes of the sites (the individual molecules), and hence their small capacitances, the charging energy dominates at room temperature. Conductivity measurements as a function of both gate bias and temperature reveal the presence of thermally activated transport, consistent with the conventional model of Coulomb blockade.

The experimental transport data available in the literature[3–8], obtained with highly ordered polycrystalline thin-film transistors (TFTs) based on α-6T and pentacene (see Fig. 1a), have so far been interpreted in terms of hopping between localized trap states, polaron hopping (both correlated and uncorrelated) or in terms of the Holstein model. However, large variations in the experimental data—on even nominally identical samples—limit the understanding of the intrinsic charge transport mechanisms of these systems.

Our sample layout is shown in Fig. 1a. The substrate is a highly doped silicon wafer, acting as a gate electrode, which is thermally oxidized in a dry atmosphere. The gold source and drain electrodes are lithographically defined, with gap diameters ranging from 2 to

20 μm. A second isolation layer is deposited to isolate the transistor electrically from neighbouring devices. The organic materials used were pentacene (Aldrich), quaterthiophene (α-4T; synthesized by Syncom BV) and sexithiophene (α-6T; also from Syncom BV). These materials were purified, and deposited in the last fabrication step by thermal evaporation in a high-vacuum environment (1×10^{-7} mbar). Large individual crystallites within a polycrystalline thin film are obtained by optimization of the substrate temperature and evaporation rate[9,10]. With optimal settings the individual crystallites can grow up to 40 μm in diameter, which is large enough to fill one gap completely, resulting in a single-crystal TFT[11]. The identification, orientation and thickness of the single crystals can be obtained by an optical polarization microscopy technique[9].

Room-temperature current–voltage (I–V) characteristics of a crystal pentacene TFT with a thin-film phase[10], measured with increasing and decreasing drain voltage, are shown in Fig. 2a. All measurements are performed under high-vacuum conditions, and as a result show little or no hysteresis in the drain voltage sweep. In contrast to what is generally reported in the literature, we typically observe non-ohmic behaviour of the gold source and drain contacts to the organic active layer[11], as is demonstrated at low drain bias in Fig. 2. The conductivity is obtained in the linear transport regime as a function of gate bias[12], and corrected for the non-ohmic contacts. A typical result is shown in Fig. 2b. The non-ohmic effects of the contacts were compensated for by measuring several sweeps of gate voltage with increasing source–drain bias ($V_d = -4, -5, -6$ and -7 V). The channel conductance at a set gate voltage is then obtained from the slope of the channel current with the applied
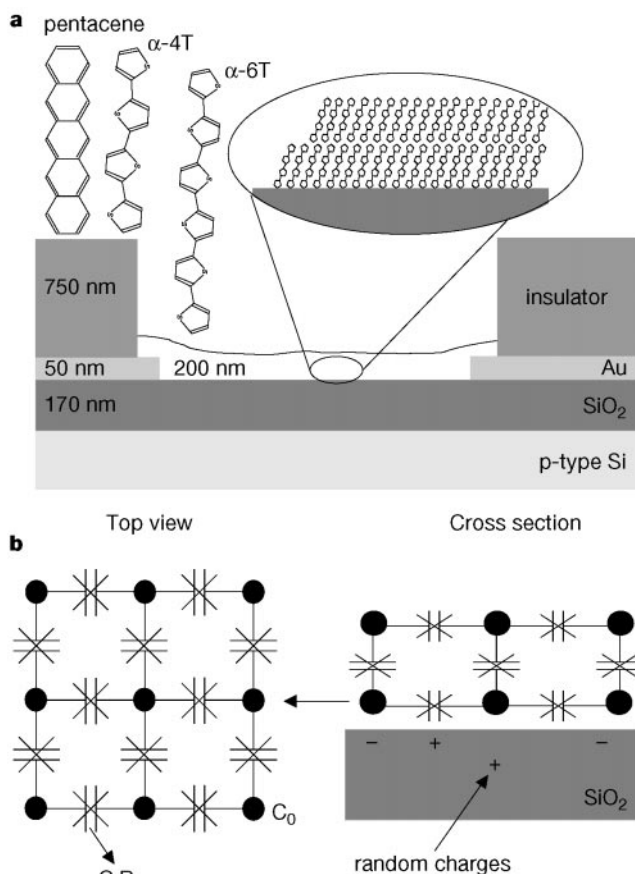
Figure 1 Schematic sample layout. **a**, Single-crystal TFT sample structure for α-4T, α-6T and pentacene materials. **b**, A schematic view of two molecular layers on top of the SiO₂ gate-dielectric with random charges incorporated. In the in-plane direction, the layers are represented by a two-dimensional array of molecules separated by a tunnel junction resistance R_T with nearest-neighbour capacitance C. The self-capacitance molecule is given by C_0.